RELIABILITY OF RADAR IMAGE DATA

by G. KONECNY and W. SCHUHR

Institute for Photogrammetry and Engineering Surveys

University of Hannover

Federal Republik of Germany

presented paper to the ISPRS '88 Kyoto-Congress

Comm. I WG 6

Abstract

Initial radar image data still is mainly slantrange or bare groundrange data. This paper deals with, how to provide geometric improved basic radar image data, which already considers ground control, digital elevation model data and sensor behavior. An introduction into basic principles of radar image geometry is followed by a report on digital methods and results, as obtained from SIR-B-, Star-1- SAR campaigns etc.
Qualitative aspects of radar image mosaics are also considered.

Keywords:
artificial ground control points, individual pixel heights, radar collinearity, radar-map, radar orthophoto.

1. Introduction

The reason for geometric (radar) image processing is, to verify the geocoding of the radar data in order to position earth surface related phenomena geometrically correct. The entire success of a radar mapping campaign depends on the ability of serious rectification of geometric distortions. Main objectives in this context are the descriptions of the steps, necessary to provide (digital) geometric precise radar maps or radar orthophotos (see Fig.4.5) in view of

- mosaiking,
- sensor comparison,
- updating etc.

This task is solved by geometric improvement of slant - as well as ground range radar image data, based upon suited projection equations, which at least allow to calculate ground control point information.

2. Radar grammetric Approaches and Results

In order to solve geometric problems for remote sensing imagery, including the radar, there are in principal the following categories of algorithms:

- image correlation (see Comm. III WG 4)
- interpolation methods
- radar blockadjustment
- combined approaches between all methods are feasible.

2.1 Interpolation methods

This are namely
- polynomial equations
- spline functions
- interpolation in a stochastic field, like
  - moving average
  - weighted mean
  - linear prediction etc.

Heuristic polynomial equations like

$$x = A_0 + A_1x' + A_2y' + A_3x'^2 + A_4y'^2 + A_5x'y'$$

and $$y = B_0 + B_1x' + B_2y' + B_3x'^2 + B_4y'^2 + B_5x'y'$$

for a SAR image of flat terrain already allow to obtain an accuracy of about ± 1 pixel, if sufficient ground control points are available.

x, y and z are terrain coordinates, x' and y' image coordinates, A_0 until B_5 are the polynomial parameters to be determined.
TRINDER archieved remarkable results for mountainous terrain by introducing a terrain-height (Z_i) depending correction term for the image ordinate values like $\Delta y_i' = K^2 \cdot Z_i / (h \cdot y'_i)$ into heuristic polynomial equations, with K_y = equivalent "focal length", h = flying altitude.

The advantages of polynomial equations are

- suited for quick programming
- satisfying for particular plane areas
- support for blunderdetection
- support for approximate value determination
- didactic introduction into geometric image processing

Some disadvantages among others are

- arbitrariness.

According to recent results of DIARRA, heuristic polynomial equations including terms depending on terrain height, for spaceborne SAR ground range imagery allow to obtain an accuracy of about ± 1 pixel. Stochastic

After treatments by
- weighted mean and
- namely by linear prediction

slightly improve this accuracy.

2.2 Radar Blockadjustment

The equations for a strict geometric approach for SAR- and SLAR-radar imagery are still a matter of research. The physical parametric solution shall allow to calculate

- the global and local behaviour of the sensor in position and attitudes
- consideration of ground control point in formation and
- changing in terrain heights for mountainous terrain.

For radar space resection the following extended equivalent collinearity equations are valid for three dimensional cartesian coordinates of a uniform reference system:

For the abscisses values follows:

$$0 = -k_x \frac{a_{11j}(x_i - DELTAX - x'_{oj}) + a_{12j}(y_i - DELTAY - y'_{oj}) + a_{13j}(z - z'_{oj})}{a_{31j}(x_i - DELTAX - x'_{oj}) + a_{32j}(y_i - DELTAY - y'_{oj}) + a_{33j}(z - z'_{oj})}$$

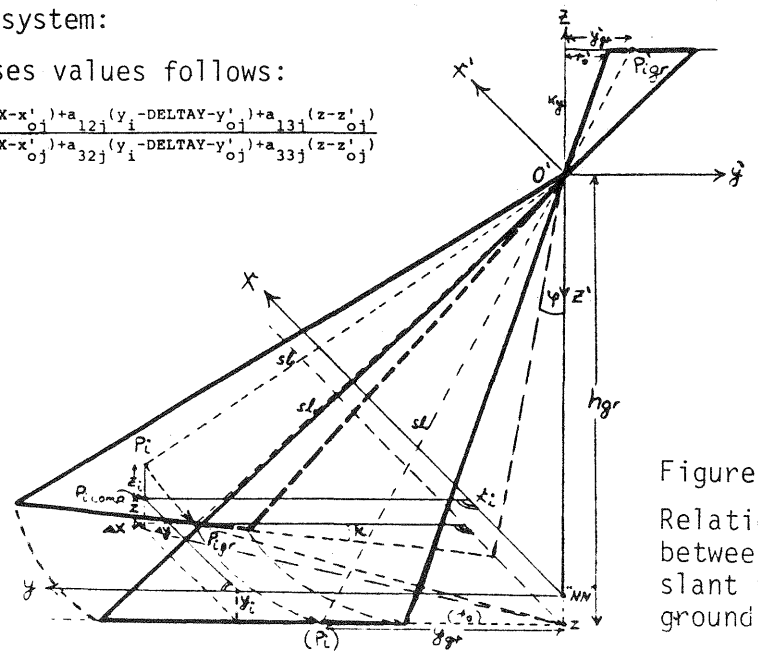

Figure 2.1:
Relation ship between slant range (sl) ground range (gr)

This is a condition equation which defines the projection within one image line. For the ground range ordinates y'_{gr} follows:

$$y'_{gr} = -k_y \frac{a_{21j}(x_i - DELTAX - x'_{oj}) + a_{22j}(y_i - DELTAY - y'_{oj}) + a_{23j}(z - z'_{oj})}{a_{31j}(x_i - DELTAX - x'_{oj}) + a_{32j}(y_i - DELTAY - y'_{oj}) + a_{33j}(z - z'_{oj})} \quad ;$$

$$DELTAX \approx \frac{((x_i - x'_{oj})^2 + (y_i - y'_{oj})^2)^{1/2} - ((x_i - x'_{oj})^2 + (x_i - x'_{oj})^2 + (y_i - y'_{oj})^2 - h^2)^{1/2}}{((x_i - x'_{oj})^2 + (y_i - y'_{oj})^2)^{1/2}} (x_i - x'_{oj})$$

$$= F \cdot (x_i - x'_{oj}); \quad DELTAY \approx F(y_i - y'_{oj})$$

with

x_i, y_i, z_i = point coordinates

$x'_{oj}, y'_{oj}, z'_{oj}$ = instantaneous sensor positions

z = terrain height chosen for the ground range processing

$h = z'_{oj} + z$; k_x, k_y = equivalent focal length,

where the instantaneous rotation-coefficients a_{11j} to a_{33j} depend on constant roll and time depending pitch and yaw values:

$$y' = y'_{gr} - r_o'$$

for slant range ordinates

$$y'_{sl} = (y'^2_{gr} + k_y^2)^{1/2}$$

$$\omega_j = \omega_o$$

$$\phi_j = \phi_o + \phi_1 x'_i + \phi_2 x'^2_i + \ldots$$

$$\kappa_j = \kappa_o + \kappa_1 x'_i + \kappa_2 x'^2_i + \ldots$$

$$x'_{oj} = x'_{oo} + x'_{o1} x'_i + x'_{o2} x'^2_i + \ldots$$

$$y'_{oj} = y'_{oo} + y'_{o1} x'_i + y'_{o2} x'^2_i + \ldots$$

$$z'_{oj} = z'_{oo} + z'_{o1} x'_i + z'_{o2} x'^2_i + \ldots$$

This expressions are valid for the general formulation of SLAR- and SAR-image geometry.
While deviations in positioning directly effect the SAR image geometry, changes in housekeeping roll, pitch and yaw do not show this kind of influence.

From the space resection equations the linearized collinearity result for second order variations in orientation elements after the elimination of high correlated terms and transition to ground coordinates:

$$dx' = -\frac{K_x}{h} y_i \, d\kappa_o - \frac{K_x^2}{h^2} y_i x_i d\kappa_1 - \frac{K_x^3}{h^3} y x_i^2 d\kappa_2 - K_x d\phi_o - \frac{K_x^2}{h} x_i d\phi_1 - \frac{K_x^3}{h^2} x_i^2 d\phi_2 - \frac{K_x}{h} dx_i$$

$$d'_y = \frac{K_y}{h} dy'_{oo} + \frac{K_y^2}{h^2} x_i dy'_{o1} + \frac{K_y^3}{h^3} x_i^2 dy'_{o2} + \frac{K_y}{h^2} y_i dz'_{oo} + \frac{K_y^2}{h^3} y_i x_i \, dz'_{o1} + \frac{K_y^3}{h^4} y_i x_i^2 dz'_{o2}$$

$$- \frac{K_y}{h} dy_i + \frac{K_y}{h^2} y_i dz - \frac{y K_y}{h^2} dz_i$$

According to BAKER (1975) the linearized collinearities allow to express equivalent polynomials, valid for ground range SLAR and SAR image geometry:

$$v'_x = a_o + a_1 y + a_2 x + a_3 xy + a_4 x^2 + a_5 yx^2 + a_6 dx_i - x'_{meas}$$

$$v'_y = b_o + b_1 y + b_2 x + b_3 xy + b_4 x^2 + b_5 yx^2 + b_6 dy_i + b_7 \cdot y \cdot dz_i - y'_{meas}.$$

where

$a_o = -K_x d\phi_o$

$a_1 = \frac{K_x}{h} d\kappa_o$

$a_2 = -\frac{K_x^2}{h} d\phi_1$

$a_3 = -\frac{K_x^2}{h^2} d\kappa_1$

$a_4 = -\frac{K_x^3}{h^2} d\phi_2$

$a_5 = -\frac{K_x^3}{h^3} d\kappa_2$

$a_6 = -\frac{K_x}{h}$

$b_o = \frac{K_y}{h} dy'_{oo}$

$b_1 = \frac{K_y}{h^2} dz'_{oo} + \frac{K_y}{h^2} dz$

$b_2 = -\frac{K_y^2}{h^2} dy'_{o1}$

$b_3 = +\frac{K_y^2}{h^3} dz'_{o1}$

$b_4 = -\frac{K_y^3}{h^3} dy'_{o2}$

$b_5 = -\frac{K_y^3}{h^4} dz'_{o2}$

$b_6 = -\frac{K_y}{h}$

$b_7 = K_y / h^2$

For third order variation in the sensor behaviour the resulting observation equations are

$$v'_x = a_o + a_1 y + a_2 x + a_3 xy + a_4 x^2 + a_5 yx^2 + a_7 x^3 + a_8 yx^3 + a_6 dx_i - x'_{meas.}$$

$$v'_y = b_o + b_1 y + b_2 x + b_3 xy + b_4 x^2 + b_5 yx^2 + b_8 x^3 + b_9 yx^3 + b_6 dy_i + b_7 \cdot y\, dz_i - y'_{meas.}$$

This approach can be extended by additional parameters to fit smoother to the ground control point field.
In comparison to heuristic polynomials arbitrariness is overcome.
For a SAR-580 ground range scene of the SIR-B semi super test site Freiburg (FRG), the strict collinearity approach has been applied onto ground control points. The resulting accuracy was about ± 10 m, see the vector diagram of Fig. 2.3 and KONECNY (1984 a).

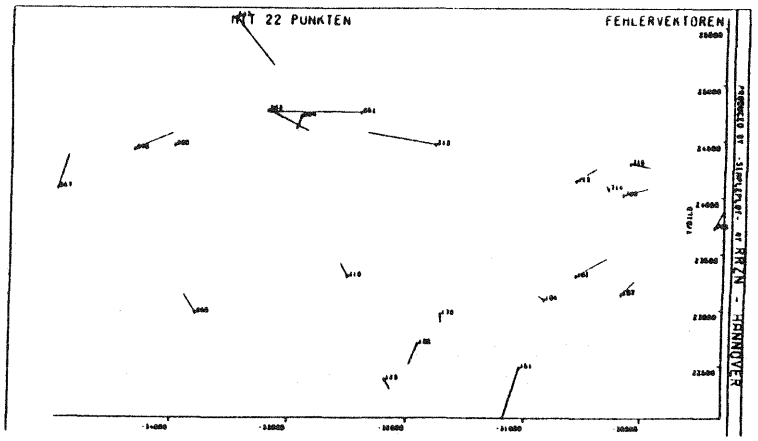

Fig. 2.3:

Residuals after applying the collinearity approach (scale abou t 1 : 50 000)

To use the advantage of existing bundle block adjustment programs for conventional photography, an approximate transformation of the radar geometry into the conventional geometry and vice versa also successfully has been carried out. This was accompanied by suited program modifications,

in order to calculate variable sensor positions and dynamics in sensor attitudes by additional parameters

The BINGO-program of the Institute for Photogrammetry according to KRUCK et al (1986) for 47 ground control points allowed to obtain an accuracy of about ± 2,5 pixels for a SIR-B image, as carried out by WIGGENHAGEN, see Fig. 4.4 and 4.5. For model coordinates differences in terrain heights Δh derived from parallaxes ΔP_y approximately result in

$$\Delta h = \frac{\Delta P_y}{b\ h} (y^2 + y \cdot b)$$

2.3 Combined Approaches

This solution has been successfully carried out for the Seasat test area Geneva. For ground control points the calculation of terrain height influences was followed by a plane polynomial approach.

After this adjustment the individual terrain heigt distortions for, e.g. unknown ground control points and every pixel have to be calculated.

Supposing roll-,pitch-and yaw-values are neglectable and under the condition of object coordinates to be transformed parallel to the image coordinate system, the following approach approximately is valid (see Fig. 4.3)

$$x'_{A_1} = x'_1 + K_x \left(\frac{X_A}{h} - \frac{x_1}{h}\right)$$

$$y'_{A_1} = y'_1 - K_y \left(\frac{y_A - \Delta y_A - y'_{oA}}{z - z'_{ol}} - \frac{y_1 - \Delta y_1 - y'_{ol}}{z - z'_{ol}}\right) \qquad \text{with} \qquad \Delta y_i = \frac{h \cdot z_i}{y_i - y_{oj}}$$

In x'_A and y'_A the index "1" indicates the unknown image coordinates (as well as later the pixel coordinates, see chapter 4.2) for the known object coordinates of point A, derived relatively to point 1, which occasionally is next to point A. The results improve by repeating the approach for approximately determination of image coordinates replacing the particular next ground control point by the second next, third next etc.

From this, new image coordinate pairs (x'_{A2}, y'_{A2}) (x'_{A3}, y'_{A3}) etc. result, which theoretically should be identical with x'_{A1}, y'_{A1}).

To realize a uniform image coordinate pair a weighted mean approach is suggested:

$$x'_A = \left(\sum_{i=1}^{i=n} (x'_{A_i} \; P_{x_i})\right) / \left(\sum_{i=1}^{i=n} P_{x_i}\right) \qquad \text{with} \qquad P_{x_i} = (x_i - x_A)^{-2}$$

$$y'_A = \left(\sum_{i=1}^{i=n} (y'_{A_i} \; P_{y_i})\right) / \left(\sum_{i=1}^{i=n} P_{y_i}\right) \qquad P_{y_i} = (y_i - y_A)^{-2}$$

or similar expressions.

This method needs a great amount of ground control points, which could be derived from densification by e.g. radar bundle block adjustment.

3. Ground Control Points

The geometrically rectified initial image data are based upon ground control point coordinates. Two categories of ground control points serve for this purpose:
- natural points, e.g. bridges, small ponds etc. and
- artificial points, like passive corner reflectors, active radar calibrators and compact receivers.

Manual ground control point extraction is susceptible to errors and tedious.

In particular for radar images with their characteristic radiometry and distortions it is extremely difficult to detect ground control points in images of mountaineous terrain. Therefore automatically or interactive ground control point extractioan and correlation methods promise a great future. Possible data sources for this procedure are digitized MC or LFC scenes, LANDSAT MSS or TM data, SPOT scenes, maps or radar imagery.

For SAR image evaluation purposes it will be necessary, to adapt the contrast of these images by filtering, smoothing and/or edge enhancement etc. Additional information is needed to calculate the scale and orientation of the GCP chips with respect to a suibable coordinate system.

The data format and the extraction process have been defined within the proposed GCP data bank which will include different data access methods, processing steps and a potential for updating.

Artificial ground control points as used by HARTL and SIEBER, mainly applied for radiometric calibration purposes, also allow precise geometric investigations.
To detect these signals in the SAR image, the test field pattern has been drawn on a transparency and connected with the radar ground range image (see Fig. 3.1. To improve this method, natural ground control points are measured in the radar image and in the map, to determine the transformation parameters. Applying this knowledge onto the three-dimensional coordinates of the mounted ground signals allows the derivation of a more precise pattern to detect the artificial points in the image, which especially succeeds digitally.

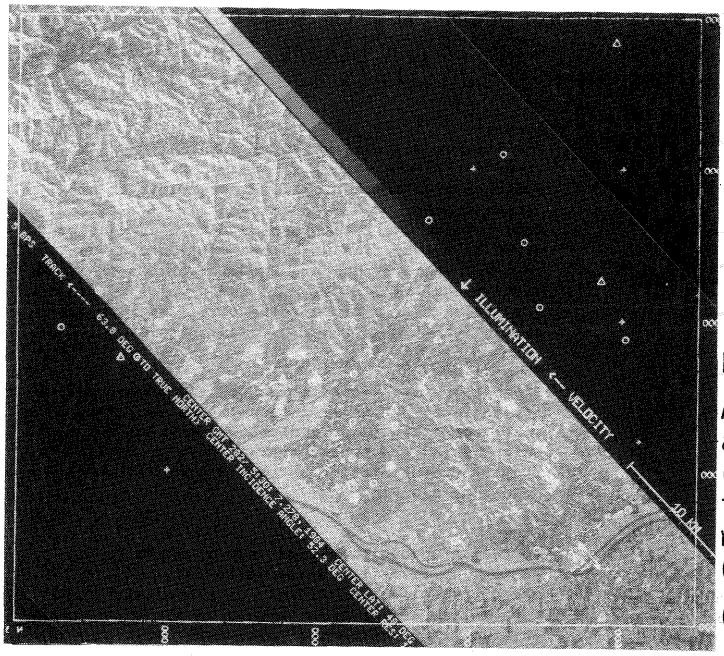

Fig. 3.1:
Approximate situation of artificial ground contol points (circles = corner refelctors, triangles = ARCS and compact receivers) in a SIR-B image (processed by DFVLR WT-DA)
(scale 1 : 500 000)

4. Radar Maps and Radar Orthophotos

4.1 Quicklook results

The proposed SAR image standard product is ground range imagery. These data might be sufficient for

- oceanographic purposes (imagery without GCPs) and
- for users in coastal areas and in flat terrain.

Fig. 4.1 shows an overlay of a spaceborne ground range image (courtesy JPL/Pasadena) with contour lines (approximate scale 1 : 500 000). The Topographic Analysis System Hannover (TASH) was applied to plot a part of the 50 m-DEM data with a 50 m contour interval. The contour lines have been appoximated by a 5th order spline function.

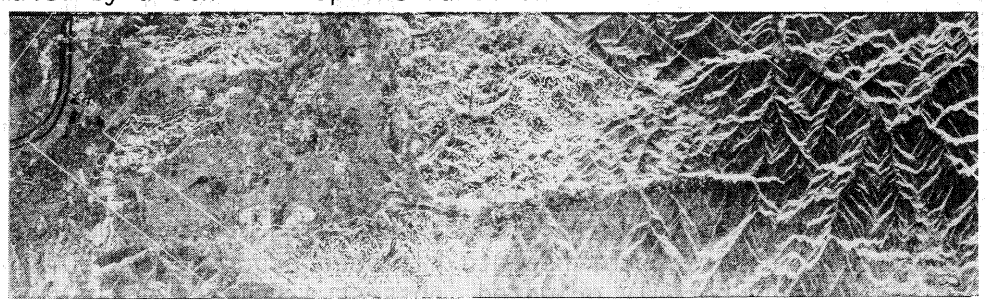

Fig. 4.1: Combination of a radar ground range image and contour lines (scale about 1 : 500 000)

4.2 Radar orthophoto

For tasks which require map accuracy (usually about ± 1 ... 3 pixels, see DOYLE (1975) and KONECNY et al. (1984 b),

- mosaiking
- multisensor imagery and
- change detection

a digital geometric pixel by pixel image restitution is needed, preferably applying the indirect rectification method, which is just in an improving phase, see Fig. 4.3.

To handle larger output image blocks and to calculate for regional or

even particular pixelwise terrain heights, according to suggestions of EGELS, MASSOU D'AUTUME of the IGN/Paris and KONECNY (1985) the following method for digital rectification has been established, see Fig. 4.3.

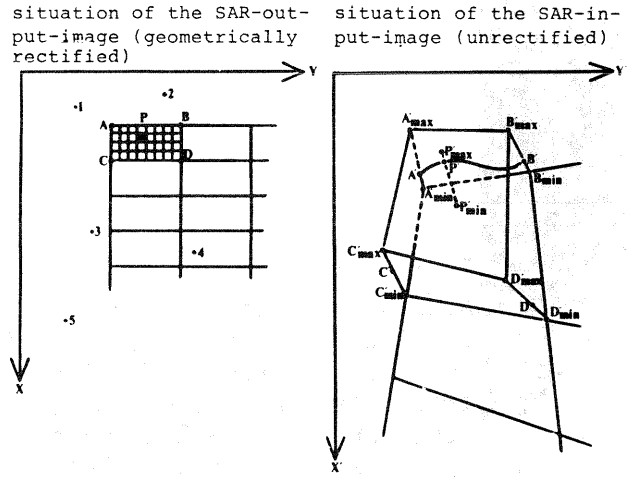

1...5 etc. = ground control points.
A...D etc. = anchor points
Small squares stand for individual pixels

every point is situated within the image plane
A'_{min}...D'_{min}, P'_{min} etc., resp.
A'_{max}...D'_{max}, P'_{max} etc., resp.
A'..D', P' = image coordinates for minimum respectively maximum respectively correct terrain height

Figure 4.3:

Calculating of individual pixel heights within an anchor point block

Step 1)
For minimum and maximum terrain height the SAR image coordinate values x' and y' of the anchor pionts are determined using a parametric or non-parametric approach (see chapter 2).
From introducing this approach onto every anchor point A, B etc., for which the map coordinates (x_A, y_A) etc. a priori are known, two sets of image coordinates ($x'_{A\ min}$, $y'_{A\ min}$) and ($x'_{A\ max}$, $y'_{A\ max}$) etc. result for minimum respectively maximum terrain height (z_{min} or z_{max}), see Fig. 4.3

Step 2)
The proper image coordinates for the anchor points are achieved by linear interpolation in between the image coordinates for minimum and maximum terrain height using the actual terrain height, derived from DEM interpolation as the argument for interpolation, see Fig. 4.3

Step 3)
For advantageous pixelwise terrain elevation calculation, at first the image coordinates x', y' for the output pixel coordinates x, y are calculated for minimum and maximum terrain height by bilinear interpolation within the particular image pixel block represented by 4 anchor points.

Step 4)
The proper image coordinates for the output pixels are computed by linear interpolation in between the image coordinates for minimum and maximum terrain height using the actual DEM-terrain height as the argument for interpolation, see Fig. 4.3

The derived orthophoto may also be generated with a digitally determined coordinate grid and edge or gradient enhancement procedures may be utilized to generate a quasi line map.

Fig. 4.4 shows a spaceborne ground range SAR image. The digital data are of courtesy of the JPL/Pasadene and the DFVLR (Oberpfaffenhofen) and have been processed by the OPTRONICS P1700 device of the Institute for Photogrammetry in Hannover.

This type of imagery is a typical product, delivered by the data acquisition facility.

Especially in mountaineous regions for a successful applying of radar data by different users a new standard product according to the sample in Fig. 4.5 is suggested. This radar orthophoto has been processed by LOHMANN. The digital data, already northly oriented, possess a uniform scale (of about 1 : 200 000). The DEM-influences are already rectified, as well as changes in the attitudes, see also SCHROEDER et al. (1985).

5. Qualitative Aspects

Due to relative low resolution, for topographic mapping purposes radar missions should concentrate on permanently clouded areas. According to ULABY the equivalent photographic pixel size for, e.g. 10 m radar resolution for 5 looks is approximately 20 m. The comparison of a radar image (Fig. 5.1) and a conventional aerial photography of the same area gives an idea of the superiority of aerial photography for topographic detail interpretation.

Fig. 4.4: Spaceborne SAR ground range image of the Freiburg test site (approximate scale 1 : 200 000)

Figure 4.5: Radar orthophoto (approximate scale 1 : 200 000)

Fig. 5.1: S AR image part (12 m pixel size)

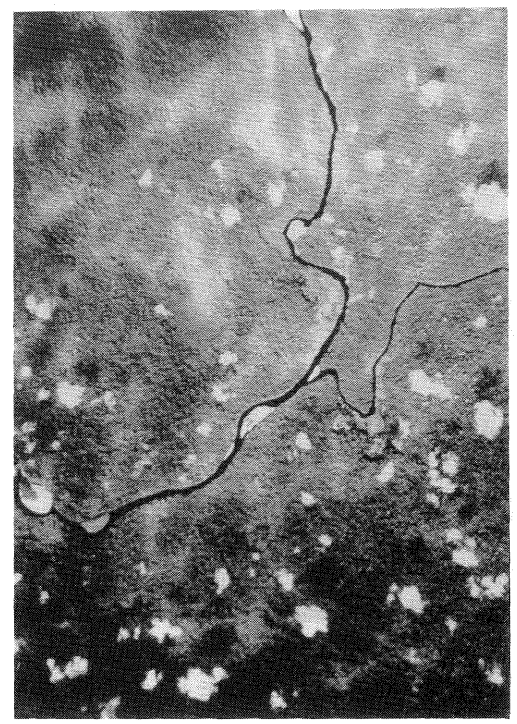

Fig. 5.2: Part of an aerial high altitude IR image of the same area

Preferable high resolution radar should be flown (see comparison between Fig. 5.3 and 5.4).

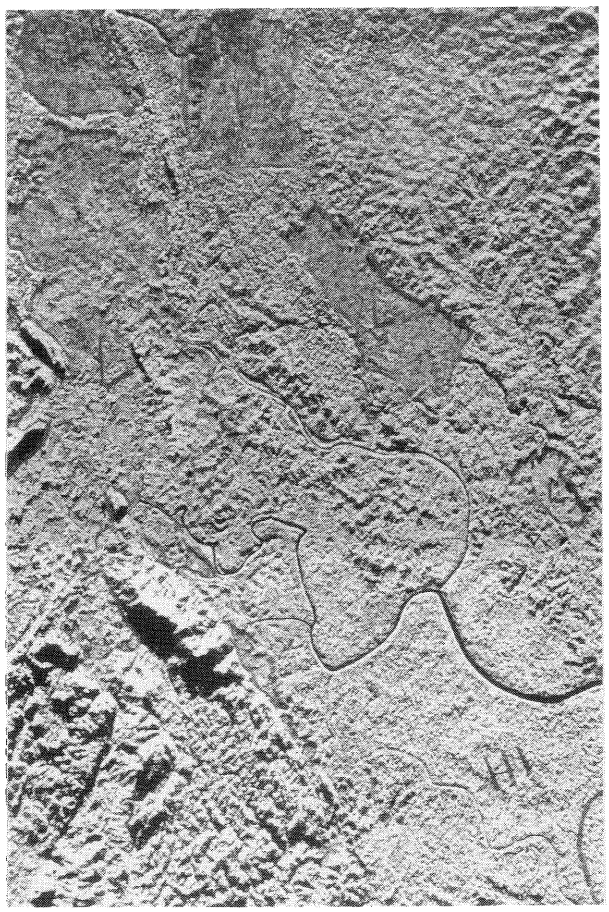

Fig. 5.3: Appr. 12 m radar resolution

Fig. 5.4: approx. 6 m radar resolution

The look direction has to be chosen with respect to topography, taking into account the final presentation in the map (notice the pseudo relief effect in figure 5.6).
In order to overcome radar shadow, opposite side look direction radar in addition to same side stereo radar should be promoted.
Figure 5.5 and Figure 5.6 show the comparison of an airborne and a spaceborne radar image with different look directions and approximately 12 m resolution over the same area.

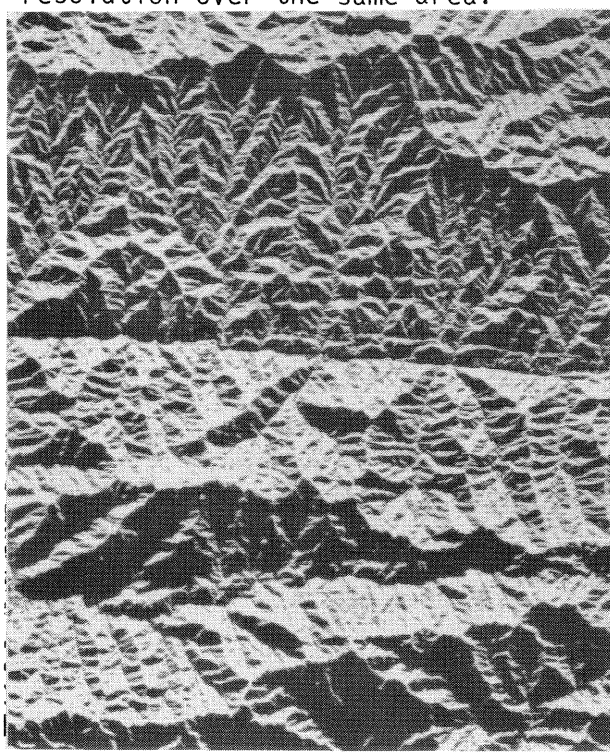

Fig. 5.5: Airborne SAR image

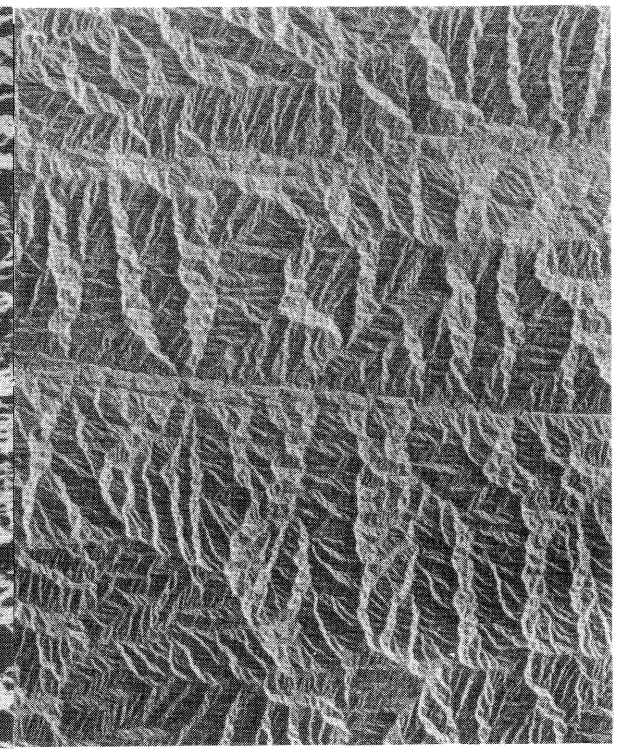

Fig. 5.6: Spaceborne SAR image

For mosaiking purposes the acceptable depression angle for image parts used in the mosaic in particular depends on the topography. The geometric approach used should follow the radar projection laws and not empiric formulations, like arbitary polynomial equations. For the future in this field a great change is expected.

For areas with lack of ground-control the radar mosaic can overcome this gap. If this gap extends one stripwidth, the polynomial parameters used for an image to image registration, due to the error propagation should be of first order.

6. REFERENCES

Baker, S.R. and Mikhail, E.M., 1975: Geometric Analysis and Restitution of Digital Multispectral Scanner Data Arrays, *The LARS, Purdue University* West Lafayette, Indiana.

Doyle, F., 1975: Cartographic Presentation of Remote Sensor Data, *Manual of Remote Sensing*, pp. 1077-1106.

Konecny, G., Schuhr, W., Engel, H., Lohmann, P., 1984: Topographic Mapping from Space Borne Metric Camera Imagery, *International Arch. for Photogrammetry and Remote Sensing*, Vol. XXV, Part A4, pp. 157-161.

Konency, G. and Schuhr, W., 1984: Practical Results of Geometric SAR-580 Image Evaluation, *International Arch. for Photogrammetry and Remote Sensing*, Vol. XXV, Part A3.

Konency, G., Schuhr, W., Engel, H., Lohmann, P., Schüring, A. and Wu, J., 1984: Investigation of Metric Camera Data Quality, *International Arch. for Photogrammetry and Remote Sensing*, Vol.XXV, Part A1, pp. 64-69.

Konecny, G., Schuhr, W., 1985: Linemap production with Metric Camera Data, *ESA Symposium Proceedings*, SP-233, pp. 69-73.

Schroeder, M., Schuhr, W. and Schüring, A., 1985: Linemapping and Resolution Tests with Metric Camera Data, *ESA Symposium Proceedings*, SP-209, pp.87-90.

Kruck, E. and Lohmann, P., 1986: Aerial Triangulation of CCD Line-Scanner Images, ESA Symposium Proceedings, (in print).